

Light scattering simulation for the characterization of sintered silver nanoparticles

Jens Hellmers^{a,*}, Norbert Riefler^a, Thomas Wriedt^b, Yuri A. Eremin^c

^aUniversität Bremen, Badgasteiner Str. 3, 28359 Bremen, Germany

^bInstitut für Werkstofftechnik, Badgasteiner Str. 3, 28359 Bremen, Germany

^cMoscow State University, Lenin's Hills, 119992 Moscow, Russia

Received 23 August 2007; received in revised form 16 October 2007; accepted 18 October 2007

Abstract

Light scattering is a useful tool in optical particle characterization. It can help to understand the nature of single particles as well as systems or clusters of particles; information about particle sizes, materials or shapes can be gathered. In this paper we investigate the application of light scattering studies to the analysis of a sintering process of silver nanoparticles. For this we first simulate the scattering behavior of two silver spheres. Then we assume sintering between them, leading to a single particle with a concave, peanut-like shape. We approximate this shape by a Cassini-oval. For light scattering studies we use an advanced T-matrix algorithm, the Nullfield Method with Discrete Sources. This method proved to be capable of simulating light scattering by concave particles. To make sure that the calculated data are correct we do comparative simulations using the Discrete Sources Method.

© 2007 Elsevier Ltd. All rights reserved.

Keywords: Nullfield Method with Discrete Sources; T-matrix; Discrete Sources Method; Nanoparticles; Silver; Sintering; Concave

1. Introduction

The special optical properties of small metal particles have been of scientific interest for a long time. The work of Gustav Mie about the optical behavior of the suspension of colloidal gold particles [1] started a development still proceeding today. Over the years a broad variety of scattering algorithms has been devised, which enabled to calculate scattering of more and more particle types and shapes in an efficient way.

In the last years nanotechnology and nanoengineering became research topics of high interest. Both terms refer to a wide field of many different investigations, approaches and applications. The knowledge of the optical properties of small particles can help to understand and predict attributes of nanoparticles. A special role in light scattering investigations was always held by small noble metal particles as they show special luminous optical properties, which are connected to shape and size. More detailed information can be found

*Corresponding author. Tel.: +49 421 2185418; fax: +49 421 2185378.

E-mail address: hellmers@iwt.uni-bremen.de (J. Hellmers).

e.g. in the paper by Gunnarsson et al. [2], the paper by Hohenester and Krenn [3] or the chapter by Burda et al. [4].

An example of an actual research field is the sintering of silver nanoparticles, because such particles show good electrical conductivity. Therefore a polymer consisting of silver nanoparticles could be used as a conducting ink, paste or glue. It was found that the electrical conductivity increases, if the silver nanoparticles are sintered, especially if they build aggregates, see e.g. the paper by Jiang et al. [5]. The question now is: can light scattering provide the information whether such particles are sintered or not—or can it even give information about the stage of the sintering process? Simulation of the light scattering process can help to get an estimation.

For this it is necessary to know the particle shapes resulting of the sintering process. A detailed investigation of the sintering mechanism of two spheres can be found e.g. in the paper of Shimosaka et al. [6]. The particle shape presented in this paper can be described as two spheres with a distinct, curved neck as connection between them and therefore reminds of the shape of a peanut. For light scattering investigations this means that it is a single particle with an aspect ratio about 2:1 and a concavity at the waist. This shape is definitely different to approaches using two spheres touching each other, two overlapping spheres or even spheroids. Therefore such particles might be not good enough as shape approximations.

In this paper we investigate light scattering by four different types of particles. We calculate scattering diagrams for two well separated silver spheres, the same spheres touching each other, an elongated single particle representing a sintered state of the two spheres and finally a more compact sintered state of the two spheres. The sintered particles with their peanut-like shapes are modeled by a Cassini-oval approach, resulting in a well fitting shape comparable to the results of Shimosaka et al. [6]. We intend to find out, whether there are any distinct differences in the scattering spectra and whether this allows to make assumptions about the state of the sintering process from light scattering. Additionally we can check, if two spheres touching each other are suitable to model a sintered particle. Corresponding, elaborated investigations of the optical behavior of such clustered nanoparticles can be found for example in the publications by Garcia de Abajo [7] or Felidj et al. [8], which give good insights into the effects caused by aggregation.

For light scattering simulation we use the Nullfield Method with Discrete Sources (NFM-DS) [9], an advanced T-matrix algorithm. To check the quality of our results calculations with the Discrete Sources Method (DSM) [10] are done.

2. Nullfield Method with Discrete Sources

The Nullfield Method (NFM), which is also known as the extended boundary condition method, is based on the work by Waterman [11]. This method allows to calculate the T-matrix, which contains all information about the scattering process. With the T-matrix further investigations like varying the direction of the incident light or orientation averaged scattering calculations can be done easily. The conventional NFM is restricted to nearly spherical particle shapes—for strongly deformed particles the NFM shows instability due to a necessary matrix inversion process and the need for finite series expansions [12]. Therefore several modifications and improvements were introduced to overcome this problem. A comprehensive overview of the available T-matrix publications can be found in the publications by Mishchenko et al. [13,14]. The NFM-DS is such a modification; it uses distributed vector spherical wave functions instead of localized vector spherical functions for field expansion. This increases the numerical stability of the algorithm compared to the conventional T-matrix approach. In this case discrete sources are distributed along the rotational axis, as the particles we are investigating can be considered prolate and axis-symmetric. Additionally, the numerical stability can be increased by varying the position of the discrete sources along the rotational axis [15].

For a more detailed description of the theory of the NFM-DS we would like to refer to the book by Doicu et al. [9], which also includes a collection of Fortran programs.

The NFM-DS enables to calculate light scattering by non-trivial particles like prolate or oblate particles with very high aspect ratios up to 100:1 [16,17] or non-symmetrical particles like superellipsoids [18] or rough particles [19] and also clusters [20]. For the investigation we are going to present in this paper it is especially of interest that the NFM-DS allows to calculate light scattering by concave particles [21].

Like all T-matrix based codes the NFM-DS is an especially fast algorithm as soon as the T-matrix is known. Then scattering computations for different directions of incident light or orientation averaged scattering calculations can be done with high computational speeds. This feature can become quite useful for investigations in which theoretically and experimentally gained scattering results are compared.

3. Sintered particle shape model

3.1. Cassini-ovals

In our present work we are first and foremost interested in the light scattering behavior of sintered particles. Therefore we leave out the specific, complex mechanism behind the sintering process as this would be beyond the aim of this paper. Instead we concentrate on the particle shape described (together with the corresponding mechanisms) by Shimosaka et al. [6]. We choose Cassini-ovals as appropriate geometrical model, which can be implemented into the NFM-DS algorithm easily.

In 1680 a special set of curves was introduced by Giovanni Domenico Cassini (1625–1712), who is also known as Jean-Dominique Cassini. These curves are characterized by a constant product of the distance of two focal points. The classical Cartesian presentation of these Cassini-ovals is given by:

$$[(x - a)^2 + y^2][(x + a)^2 + y^2] = b^4. \tag{1}$$

The equivalent form depending on y is

$$y = \pm (-a^2 - x^2 \pm (4x^2a^2 + b^4)^{1/2})^{1/2}. \tag{2}$$

There is also a polar notation:

$$r^4 + a^4 - 2a^2r^2 \cos(2\theta) = b^4, \tag{3}$$

which means for r :

$$r = \pm \left(a^2 \left[\cos(2\theta) \pm \left(\frac{b^4}{a^4} - \sin^2(2\theta) \right)^{1/2} \right] \right)^{1/2}. \tag{4}$$

Alternatively, the direct substitution of (1) using $x = r \cos(\theta)$, $y = r \sin(\theta)$ and transforming it into polar coordinates $r = r(\theta)$ gives:

$$r = \pm (a^2 - 2a^2 \sin^2(\theta) \pm (-4a^4 \sin^2(\theta)^2 + 4a^4 \sin^4(\theta) + b^4)^{1/2})^{1/2}. \tag{5}$$

Therefore the shape of the Cassini-oval depends on the relation b/a . If $a < b$ the result is an oval loop, for $a = b$ the result is an lemniscate (as the ∞ -symbol) and for $a > b$ the result consists of two separated curves. Fig. 1 gives an overview of the resulting shapes.

If a is chosen slightly smaller than b , the emerging curve gets a concave, peanut-like shape; the closer a gets to b , the deeper the concavity.

Rotating such a shape around its longitudinal or major axis allows to create the wanted, three-dimensional shape for describing two sintered spheres. One problem is, that it is quite difficult to manipulate the particle

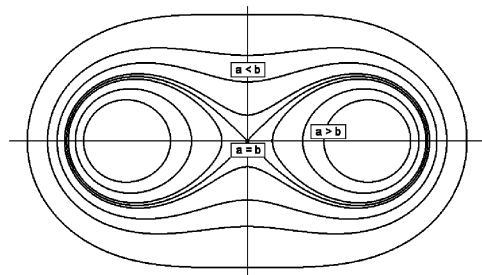


Fig. 1. Cassini-ovals for a given a and varying b .

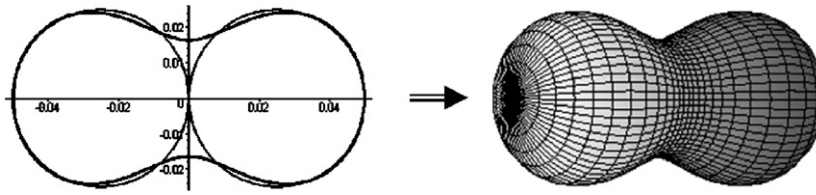


Fig. 2. Two dimensional and 3 dimensional peanut-like particle based on a Cassini-oval. The two-dimensional curve is additionally compared to two circles.

shape by varying the values for a and b . Changing one value to change the particle length also always changes the particle thickness. Therefore it is helpful to introduce another parameter c that allows to manipulate the thickness directly:

$$y = c \pm (-a^2 - x^2 \pm (4x^2a^2 + b^4)^{1/2})^{1/2}. \quad (6)$$

This makes the process of form-fitting much easier and allows to create shapes which are quite reasonable when compared to the spheres we assume as origin. Fig. 2 shows an example.

Instead of the Cassini-oval approach (or a comparable one) one could consider to use a three-dimensional grid model of the shape. This is possible, but an analytical model for shape description in the code of the algorithm significantly reduces calculation times—especially if the particle is rotational-symmetric.

In their paper Shimosaka et al. [6] describe, that different processes during sintering can have different influence on the volume. For comparable light scattering simulation results we assume a constant volume for all particles we are going to investigate; the single particle should have the same volume as the original two spheres before. The volume of such a peanut-like particle can be easily determined using the general formula for the volume of a solid of revolution

$$V = \pi \int_u^v (f(x))^2 dx, \quad (7)$$

where (6) is inserted as $f(x)$; additionally the algebraic signs and limits must be chosen accordingly.

3.2. Investigated particles

In this work light scattering by silver nanoparticles in different stages of the sintering process is investigated. First, we consider two single, separated spheres. Then the gap is closed so that the two spheres touch each other in one point. In the next step the particles start to sinter and become one particle; a Cassini-oval approach is used to describe the resulting shape. The Cassini-parameters are chosen in such a way, that the particle is still very much sphere-like at the outer rim and it is made sure, that the volume of the single particle is equivalent to the volume of the two spheres before. For the sintered particle we investigate light scattering for two cases: one with particles just slightly melted together and one tighter set.

The exact values are as followed:

- (1) Two separated spheres; sphere diameter (both) = $0.05 \mu\text{m}$, distance between the centers = $0.07 \mu\text{m}$.
- (2) Two spheres touching each other in one point; sphere diameter (both) = $0.05 \mu\text{m}$.
- (3) Cassini-oval; $a = 0.0340625$, $b = 0.0365625$, $c = 1.236$. This leads to a particle with a length of $0.0999 \mu\text{m}$, a maximum thickness of $0.0485 \mu\text{m}$ and a minimum thickness of $0.0328 \mu\text{m}$. The diameter of two equivalent spheres differs just about 0.0013% from the original $0.05 \mu\text{m}$.
- (4) Cassini-oval; $a = 0.0307$, $b = 0.035$, $c = 1.21$. This leads to a particle with a length of $0.0931 \mu\text{m}$, a maximum thickness of $0.0483 \mu\text{m}$ and a minimum thickness of $0.0407 \mu\text{m}$. The diameter of two equivalent spheres differs just about 0.0017% from the original $0.05 \mu\text{m}$.

Fig. 3 gives an impression of the corresponding shapes.

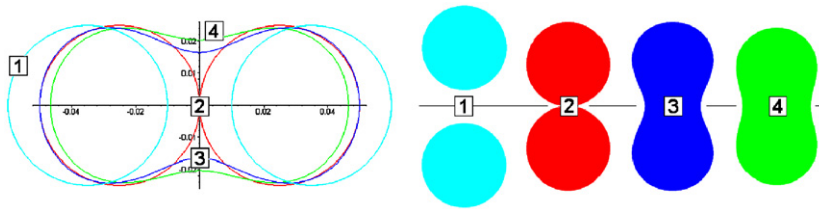


Fig. 3. Particles investigated in this paper.

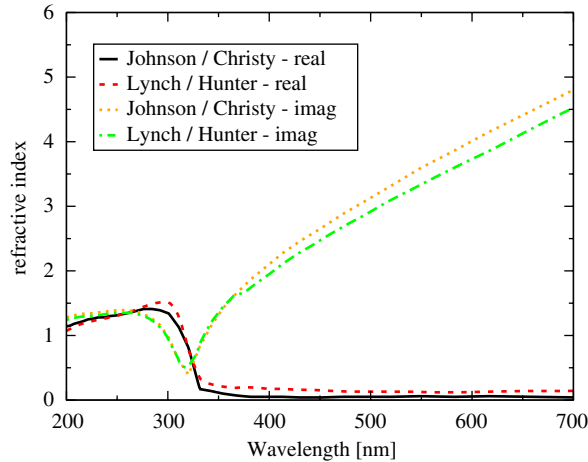


Fig. 4. Refractive index of silver. Data given by Johnson and Christy [23] compared to data given by Lynch and Hunter [24].

4. Refractive index of silver

The refractive index of silver strongly depends on the wavelength. Over the years there have been a lot of investigations regarding to this topic. Naturally the gathered data are not consistent, the values differ—depending for example on the state of the measured silver like massive, vaporized or sprayed. Tables with measured data can be found e.g. in the Landolt–Börnstein collection [22]. Over the years the publications by Johnson and Christy [23] on one side and Lynch and Hunter [24] on the other side have become especially popular and a kind of standard, also because they offer data for a wide wavelength range. Fig. 4 gives an impression of the refractive index depending on the wavelength.

While there are differences in detail nevertheless both data sets show a similar trend. The most distinct characteristic is a strong descent in real as well as imaginary part between 250 and 350 nm, followed by a steep climb of the imaginary part. This might become obvious in a spectral analysis of the light scattering behavior—which we are going to investigate.

In our work we use the data by Johnson and Christy.

5. Simulation results

For our investigation we calculate the normalized differential scattering cross-section (DSCS) for each of the four shapes shown in Fig. 3 for a wavelength range from 250 to 700 nm in 2 nm steps. We have a look at different cases: we choose the incident direction parallel and perpendicular to the rotational axis, additionally we calculate the orientation averaged scattering patterns.

First, to ensure the accuracy of the simulations results, we exemplarily compare our results to those of the DSM. In the frame of the DSM an approximate solution of the boundary value problem is constructed as a finite linear combination of the field of dipoles and multipoles deposited in some supplementary domain.

A full review about the DSM can be found e.g. in the book chapter by Eremin et al. [10]. Fig. 5 shows such an exemplary comparison for a sintered particle.

For the actual analysis in the first step all NFM-DS scattering diagrams for the incident direction parallel to the rotational axis and the orientation averaged scattering are arranged consecutively. The result is a three-dimensional presentation—see Figs. 6–9. This helps to identify significant areas with noticeable effects. The data then were analyzed further by a spectral investigation in forward direction. To get a detailed impression, we do a detector-averaged investigation. In this case detector-averaging is about 4° , which means that we average the values from 358° ($= -2^\circ$) to 2° . The results are plotted into three diagrams—see Fig. 10.

To sum up the observations we first look at the three-dimensional patterns, see Figs. 6–9: for the case of an incident direction parallel to the rotational axis all profiles show a decreasing intensity over the whole angular range for wavelengths between 250 and 320 nm. This is followed by a steep rise, leading to a peak between 360 and 370 nm. After this peak the intensity consistently decreases again. A closer look at the main peak in the scattering profiles for incident direction parallel to the rotational axis also shows a difference between the

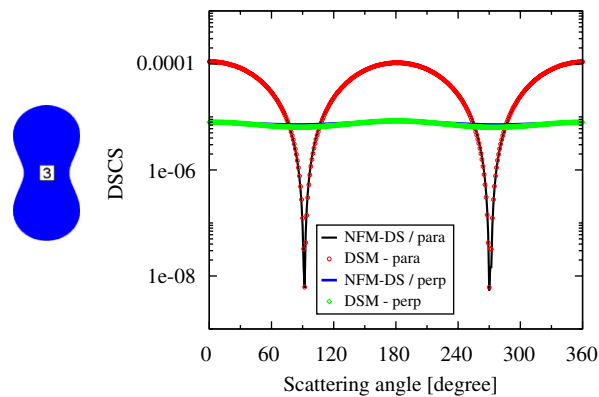


Fig. 5. Comparison of DSCS diagrams calculated by NFM-DS and DSM, parallel and perpendicular polarization. Particle shape is the Cassini-oval based peanut '3' from Fig. 3, particle length is 100 nm. Incident angle is 90° to rotational axis. Wavelength is 478 nm, corresponding refractive index is $0.13 + 2.729i$.

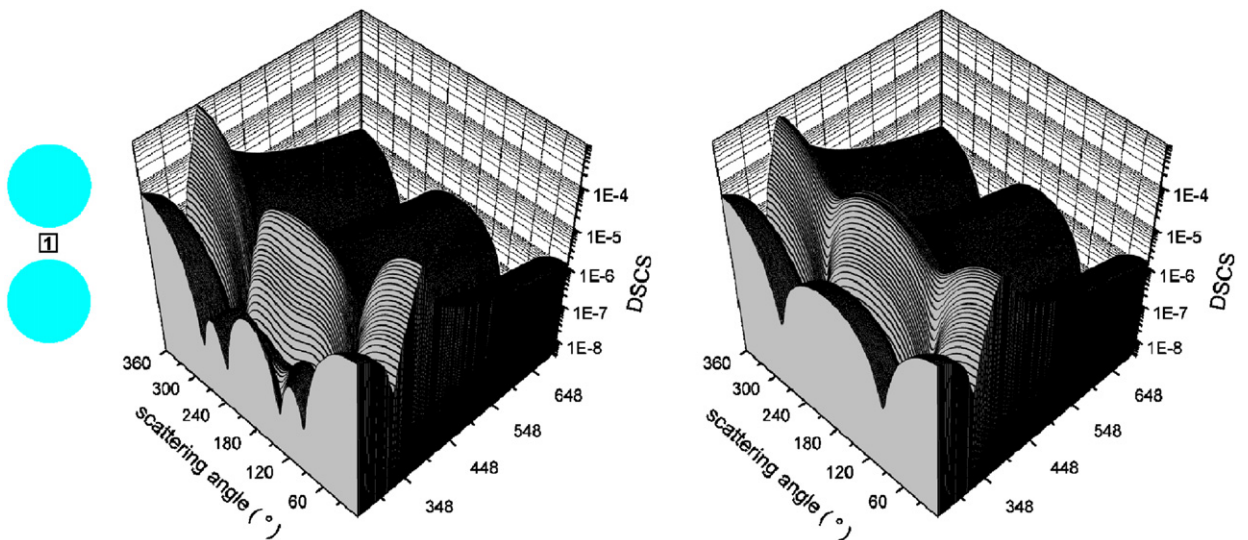


Fig. 6. Two separated spheres: three-dimensional arrangement of DSCS diagrams. Sphere diameter = 50 nm, distance between the centers = 70 nm (see Fig. 3). Left: direction of incident light parallel to rotational axis. Right: orientation averaged scattering. Wavelength range is from 250 to 700 nm in 2 nm steps with corresponding refractive indices (see Fig. 4). Shown is parallel polarization.

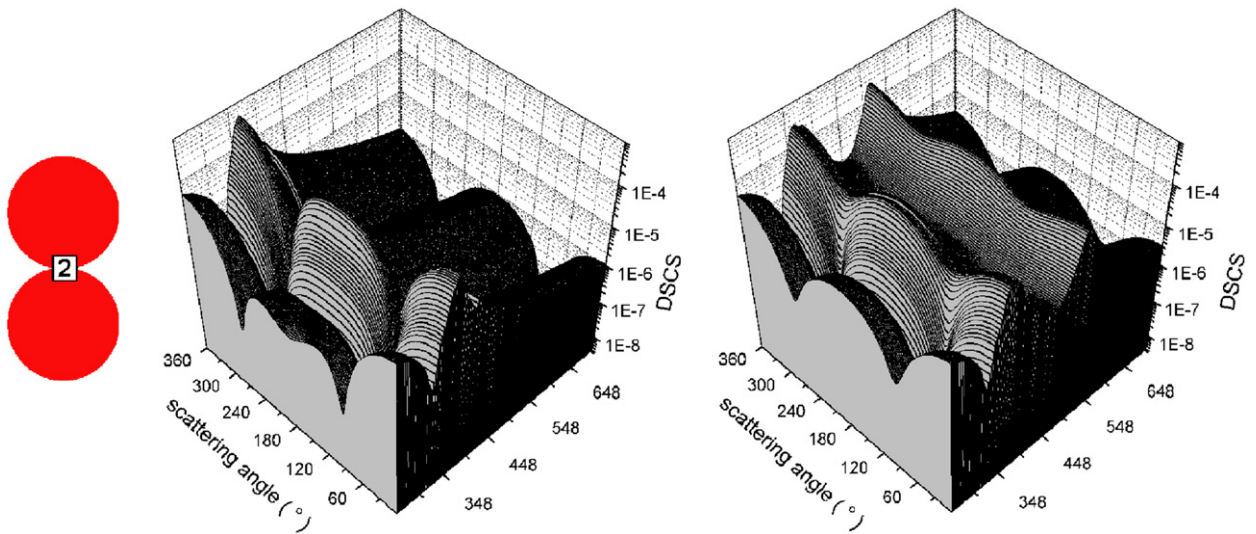


Fig. 7. Two spheres touching each other: three-dimensional arrangement of DSCS diagrams. Sphere diameter = 50 nm (see Fig. 3). Left: direction of incident light parallel to rotational axis. Right: orientation averaged scattering. Wavelength range is from 250 to 700 nm in 2 nm steps with corresponding refractive indices (see Fig. 4). Shown is parallel polarization.

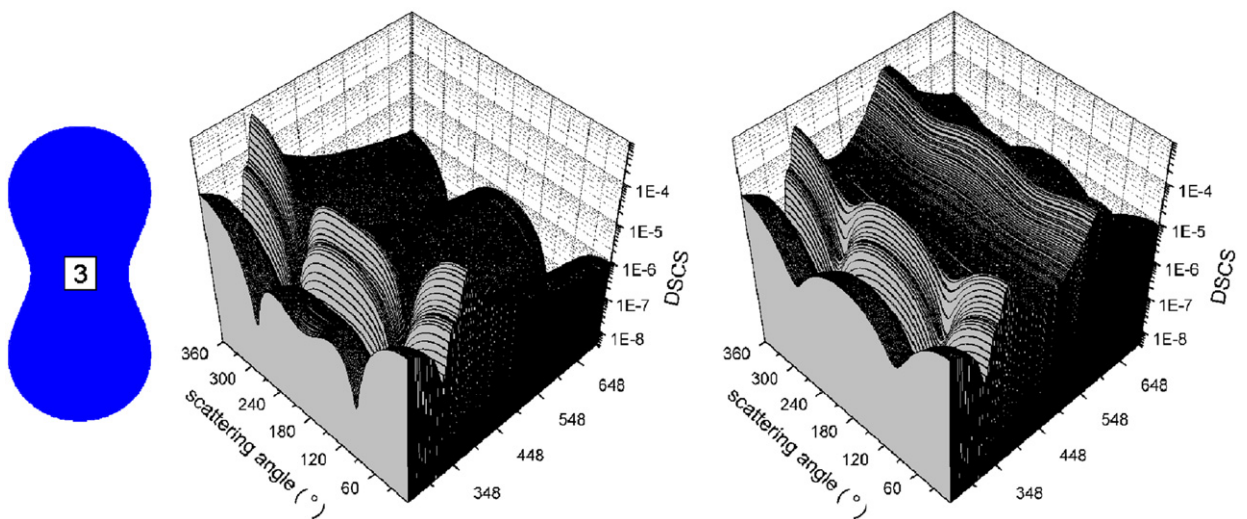


Fig. 8. Two sintered spheres: three-dimensional arrangement of DSCS diagrams. Cassini-parameters $a = 0.0340625$, $b = 0.0365625$, $c = 1.236$ (see Fig. 3). Left: direction of incident light parallel to rotational axis. Right: orientation averaged scattering. Wavelength range is from 250 to 700 nm in 2 nm steps with corresponding refractive indices (see Fig. 4). Shown is parallel polarization.

‘two-sphere’ arrangement and the ‘single-particle’ Cassini shapes: the flank of the peaks for the two spheres are smooth while it has a little step for the Cassini shapes.

Even more obvious differences can be observed from the orientation averaged scattering. With the exception of the separated spheres a second peak starting from wavelengths greater than 400 nm appears. This second peak also changes its position depending on the form of the investigated particles.

The two-dimensional diagrams in Fig. 10 show this more detailed: for the case of an incident direction parallel to the rotational axis there is just one peak for every of the particle shapes. These peaks are in the same wavelength area. The peak for the two separated spheres is the highest while the others are quite similar. If the direction of the incident light is perpendicular to the rotational axis these peaks about 360–370 nm are still

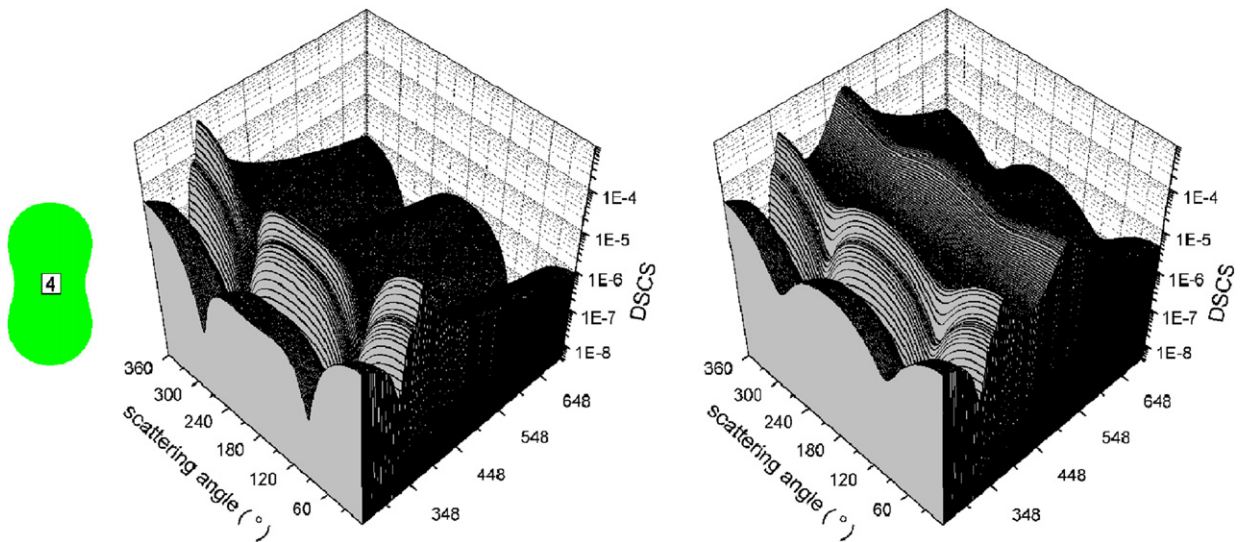


Fig. 9. Two sintered spheres: three-dimensional arrangement of DSCS patterns. Cassini-parameters $a = 0.0307$, $b = 0.035$, $c = 1.21$ (see Fig. 3). Left: direction of incident light parallel to rotational axis. Right: orientation averaged scattering. Wavelength-range is from 250 to 700 nm in 2 nm steps with corresponding refractive indices (see Fig. 4). Shown is parallel polarization.

visible, but for the Cassini-based shapes they are negligible. Instead for these two shapes a second peak appears, reaching a maximum at 550 nm for the stretched and at 480 nm for the compact Cassini shape. Also the two spheres touching each other show this second peak, here at 510 nm. The separated spheres show no such peak. In all cases the second peak is higher than the first.

The orientation averaged scattering shows a mixture of both diagrams described—as one would expect.

6. Summary and conclusion

We investigate four different particle systems, respectively particles. The scattering setup is based on a sintering process of two silver spheres. In the first step the spheres are separated. Then they touch each other. Finally sintering starts and one gets a single particle, which we model by a Cassini-oval approach and for two different stages of the process. For these particles we calculate light scattering diagrams for different incident angles and also orientation averaging is done.

Our first conclusion is, that the NFM-DS as a T-matrix based algorithm is capable of calculating light scattering by prolate, concave particles. This was demonstrated by comparing light scattering patterns by the NFM-DS to those calculated by the DSM.

For a more detailed interpretation we now would like to start by having a look at the intensity peak between 360 and 370 nm, which could be observed in all diagrams. At first one could assume, that this behavior in some respects is connected to the noticeable, steep drop of both real and imaginary part of the refractive index of silver between 250 and 350 nm, which is followed by a steep climb of the imaginary part—as it was shown in Fig. 4. This would indicate a direct connection between the peak and refractive index. Fig. 11 compares the curves from Figs. 4 and 10 (top) to give a better impression. If there is a connection, it is more likely that it is due to the steep climb of the imaginary part of the refractive index: as it reaches its minimum also the intensity in forward direction reaches its minimum. After that both start to climb with increasing wavelengths. But then the DSCS gets to a maximum and starts to drop significantly while the imaginary refractive index still climbs. So the correlation of refractive index and wavelength should not be the only reason. As another observation shows that the first peak for the two separated spheres is much higher than for the other particles, it is likely, that there is also an influence by the shape.

A second peak can be observed for incident directions deviating from parallel to the rotational axis and only if the spheres touch each other or start to sinter. This is an important fact for our investigations, because it is

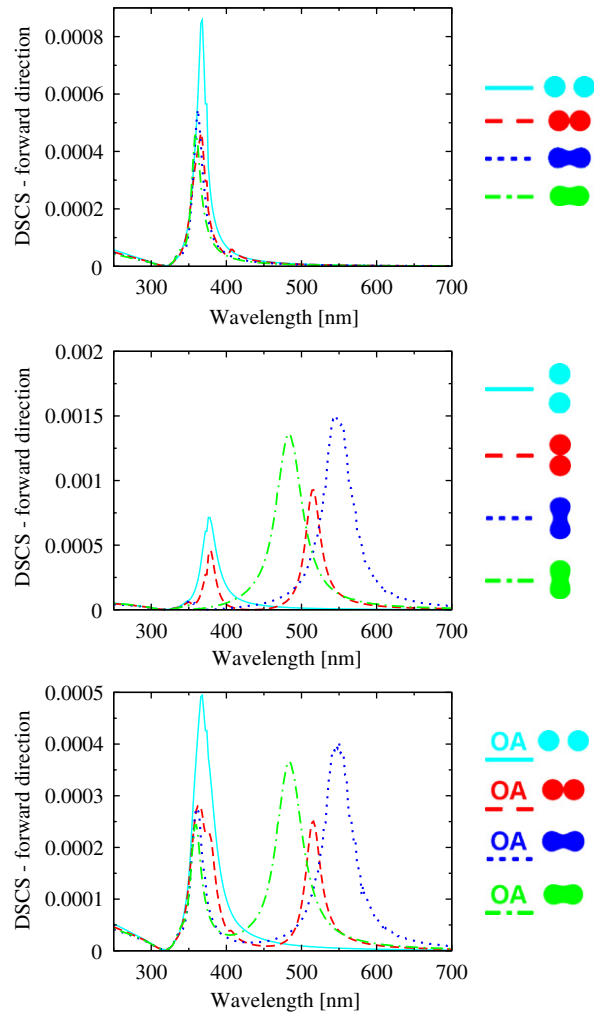


Fig. 10. Spectral analysis of the detector-averaged DSCS in forward direction. Area for detector-averaging is 4° . Wavelength range is from 250 to 700 nm in 2 nm steps. Top: incident direction parallel to rotational axis. Middle: incident direction perpendicular to rotational axis. Bottom: orientation averaged scattering.

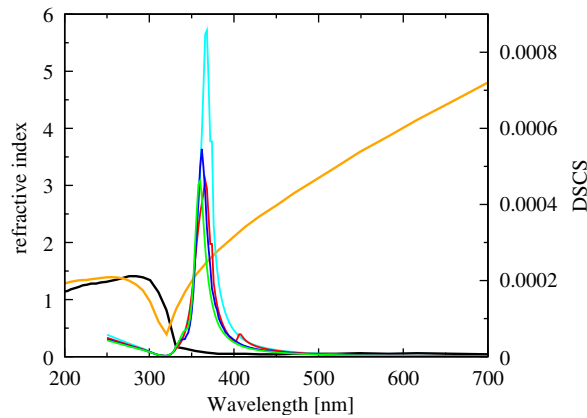


Fig. 11. Comparison: refractive indices of silver and spectral DSCS for the same wavelength range. This diagram is Fig. 4 overlaid by Fig. 10—top. Note: this diagram is just to give an impression about the position of the main peak in scattering compared to the wavelength dependency of the refractive index of silver.

reasonable to assume, that the appearance of this second peak is an indicator that the two spheres become one particle. Additionally, as the position of the second peak changes with the shape of particle, it should allow conclusions about the status of the sintering process.

The fact, that the second peak only appears for incident directions deviating from parallel to the rotational axis can be explained if one keeps in mind, that all the particles, respectively particle systems, investigated here look the same from that direction; an observer would only see a spherical shape.

To sum it up, all four different particle systems, respectively particles, show a different scattering behavior. These differences are significant, so that it should be possible to differ between the particles. Particularly it should be possible to decide, if an observed particle is sintered or not. It might be even possible to determine the stage of the sinter process, especially as the two separated spheres show a considerably varied scattering behavior for the orientation averaged case. Of course these observations primarily are valid just for 0.05 μm particles. But because of the satisfying results further investigations for silver spheres of different diameters look promising as well.

Acknowledgment

We would like to acknowledge support of this work by Deutsche Forschungsgemeinschaft DFG.

References

- [1] Mie G. Beiträge zur Optik trüber Medien, speziell kolloidaler Metallösungen. *Annalen der Physik* 1908;4(25):377–445.
- [2] Gunnarsson L, Rindzevicius T, Prikulis J, Kasemo B, Käll M, Zou S, et al. Confined plasmons in nanofabricated single silver particle pairs: experimental observations of strong interparticle interactions. *J Phys Chem B* 2005;109:1079–87.
- [3] Hohenester U, Krenn J. Surface plasmon resonances of single and coupled metallic nanoparticles: a boundary integral method approach. *Phys Rev B* 2005;72:195429.
- [4] Burda C, Green T, Landes C, Link S, Little R, Petroski J, et al. In: Wang ZL, editor. *Characterization of nanophase materials*. New York: Wiley-VCH; 2000.
- [5] Jiang H, Moon KS, Lu J, Wong CP. Conductivity enhancement of nano silver-filled conductive adhesives by particle surface functionalization. *J Electron Mater* 2005;34(11):1432–9.
- [6] Shimosaka A, Ueda Y, Shirakawa Y, Hidaka J. Sintering mechanism of two spheres forming a homogeneous solubility neck. *KONA* 2003;21:219–33.
- [7] Garcia de Abajo FJ. Multiple scattering of radiation in clusters of dielectrics. *Phys Rev B* 1999;60(8):6086–102.
- [8] Felidj N, Aubard J, Levi G. Discrete dipole approximation for ultraviolet–visible extinction spectra simulation of silver and gold colloids. *J Chem Phys* 1999;111(3):1195–208.
- [9] Doicu A, Wriedt T, Eremin Y. *Light scattering by systems of particles. Null-field method with discrete sources: theory and programs*. Berlin/Heidelberg/New York: Springer; 2006.
- [10] Eremin Y, Orlov N, Sveshnikov A. Models of electromagnetic scattering problems based on discrete sources method. In: Wriedt T, editor. *Generalized multipole techniques for electromagnetic and light scattering*. Amsterdam: Elsevier; 1999. p. 39–80.
- [11] Waterman PC. Matrix formulation of electromagnetic scattering. *Proc IEEE* 1965;53:805–12.
- [12] Mishchenko MI, Travis LD, A Lacis A. *Scattering, absorption and emission of light by small particles*. Cambridge: Cambridge University Press; 2002.
- [13] Mishchenko M, Videen G, Babenko V, Khlebtsov N, Wriedt T. T-matrix theory of electromagnetic scattering by particles and its applications: a comprehensive reference database. *JQSRT* 2004;88:357–406.
- [14] Mishchenko M, Videen G, Babenko V, Khlebtsov N, Wriedt T. Comprehensive T-matrix reference database: a 2004–06 update. *JQSRT* 2007;106:304–24.
- [15] Hellmers J, Wriedt T. Nullfield method with discrete sources: influence of the deposition of discrete sources on numerical stability. In: Voshchinnikov N, editor. *Proceedings of the ELS9, St. Petersburg, Russia; 2006*. p. 71–4.
- [16] Pulbere S, Wriedt T. Light scattering by cylindrical fibers with high aspect ratio using the null-field method with discrete sources. *Part Part Syst Charact* 2004;21:213–8.
- [17] Hellmers J, Wriedt T, Doicu A. Light scattering simulation by oblate discsphere using the Nullfield Method with Discrete Sources located in the complex plane. *J Mod Opt* 2006;53:267–82.
- [18] Wriedt T. Using the T-matrix method for light scattering computations by non-axisymmetric particles: superellipsoids and realistically shaped particles. *Part Part Syst Charact* 2002;19:256–68.
- [19] Hellmers J, Wriedt T. T-matrix light scattering simulation of rough, non-symmetrical spherical particles. *JQSRT* 2007;106:90–103.
- [20] Riefler N, di Stasio S, Wriedt T. Structural analysis of clusters using configurational and orientational averaging in light scattering analysis. *JQSRT* 2004;89:323–42.

- [21] Hellmers J, Eremina E, Wriedt T. Simulation of light scattering by biconcave Cassini ovals using the Nullfield Method with Discrete Sources. *J Opt A* 2006;8:1–9.
- [22] Hellwege KH, Hellwege AM, editors. *Landolt-Börnstein II. Band: Eigenschaften der Materie in ihren Aggregatzuständen, 8. Teil: optische Konstanten*. Berlin: Springer; 1962.
- [23] Johnson PB, Christy RW. Optical constants of the noble metals. *Phys Rev B* 1972;6(12):4370–9.
- [24] Lynch DW, Hunter WR. Comments on the optical constants of metal and an introduction to the data for several metals. In: Palik ED, editor. *Handbook of optical constants of solids, vol. 1*. San Diego: Academic Press; 1985.